Check for
updates

Modified Koch borderline monopole antenna for THz regime

Taruna Sharma[1] · Gaurav Varshney[2] · R. S. Yaduvanshi[3] · Munish Vashishath[1]

Abstract

A modified Koch frontier, super wide band antenna is designed and analyzed in both frequency and time domain. A novel combination of partial ground structure with asymmetric polygon shape patch is proposed in this letter. Higher order TM modes are excited in the structure and amalgamated in order to provide an impedance bandwidth of 139%. Average radiation efficiency of 85% is obtained throughout the resonating band of the antenna. Electrical shortening of antenna is achieved by modifying shape of patch to yield an operating bandwidth of 12.5 THz (2.7–15.2 THz) with a peak gain of 6 dBi. Furthermore, antenna behaves as monopole antenna for lower frequencies of operating bandwidth. Pulse preserving property in three direction paradigm is verified for far field radiation of the antenna and a high fidelity factor of 0.9597 is obtained. Presented antenna is best suited to be used as a terahertz (THz) pulse generator and detector in THz pulse imaging (TPI) systems for dental caries, dermatological practices, breast cancer and brain tumor detection.

Keywords Koch-fractal · THz pulse imaging · Partial ground structure

1 Introduction

Recent advancements in wireless communication technologies have totally transformed the outlook of our society towards sharing and accessing the information via wireless media (Akyildiz et al. 2014). Terahertz (THz) regime (0.1–30 THz), is now envisioned as the potential candidate to alleviate scarcity of channel capacity and channel modeling with less fading and high spectral efficiency (Koenig et al. 2013). Researchers have realized multiple devices such as modulator, power divider, filter, antenna in this least explored spectrum (Cheng et al. 2019). Among all these devices, antenna is indeed a pivotal element of every communication system to exchange information. Scientists have designed and analyzed numerous antenna structures for various applications. Some of the application includes health care and monitoring systems (Nafari and Jornet 2015; Son 2009; Grade et al. 2007), defense applications (Galoda and Singh 2007), energy harvesting (Shanawani et al. 2017;

✉ Taruna Sharma
parashar.taruna@gmail.com

1   J C Bose University of Science and Technology, YMCA, Faridabad, Delhi 121006, India

2   NIT Patna, Patna, India

3   NSUT Delhi, New Delhi 110031, India

Obayya et al. 2018), high spectral efficiency (Xu et al. 2014) and high speed applications (Goyal and Vishwakarma 2018). Major challenges encountered by this technology are high attenuation of electromagnetic waves and dearth of compact sources at such high frequency. In order to mitigate attenuation losses, several high gain structures including MEMS helix antenna (Guo et al. 2014), meta material radome (Seyedsharbaty and Sadeghzadeh 2017), 2×2 patch antenna array (Luk et al. 2017), meta material loaded patch (Denizhan Sirmaci et al. 2016), massive MIMO structures (Akyildiz and Jornet 2016) and lens antenna (Formanek et al. 2009) have been introduced. All these designs are capable enough to compensate for losses occurred in path of electromagnetic wave, but mismatching due to augmented size is still a matter of concern for antenna designers.

Patch antennas have gained immense popularity due to their planar structure and ease in fabrication for RF and microwave range. A variety of patch antennas have been derived and modeled from RF to THz range (Unal and Aksun 2015; Kucherik et al. 2019; Varshney et al. 2019) providing an implementation method to bridge the gap between RF microwave and THz technology. Reconfigurable and tunable graphene based patch antenna (Bala and Marwaha 2016; Sharma et al. 2020), with PBGhigh gain antenna (Jha and Singh 2012) have also been proposed. Various geometrical shapes including Square and rectangular geometry is analyzed in Jha and Singh (2010) and Jha and Singh (2009). Along with simple geometries, fractal geometries have also been widespread (Werner and Ganguly 2003) in RF range. A variety of nano metallic antennas have been proposed in literature which are exhibiting ultra wide band characteristics. An elliptical metallic patch antenna (Singhal 2019a) with high gain and large impedance bandwidth have proposed while (Singhal 2019b; Das et al. 2020) makes use of fractal approach to solve the problem of gain with ultra wide bandwidth. Recently graphene based patch and rectangular patch antenna with high gain characteristics have been reported for THz communication range (Das and Rawat 2021; Shamim et al. 2021). Geometry of ultra wide band antennas reported in these research articles makes use of symmetrical geometry of antenna. Geometrical aspect of nano metallic patch antennas have not been explored in asymmetrical context.

This paper presents a new approach of designing Koch curve frontier with partial ground structure to resolve the problem of super wide bandwidth along with high gain. Partial ground structure can be considered as a standard practice to increase the bandwidth in microwave spectrum (Pickwell and Wallace 2006). Koch curves are essential fragmented structures which can be described by their indentation angle. Koch curves are highly convoluted and retain possibility to bind a very large curve into a finite area (Mirmosaei et al. 2016). In this design, asymmetrical polygon shape patch antenna is designed and impedance bandwidth is increased with implementing partial ground structure to the antenna. Space filling property of this fractal antenna is utilized and modifications in the geometry of antenna are done with a triangular approach. THz radiations have coherent detection and penetrating beyond surface properties. Due to these features, refractive index and absorption coefficient of any object can be estimated. Presented structure is specifically proposed for TPI (THz pulse imaging) along with THz spectroscopy to differentiate between benign and malign tissues (Mathur and Gupta 2014). A key point that can be noted about earlier proposed designs is that geometry of all those nano antennas follows line symmetry. In this research, this is the first time a research work is reported, which optimize geometrical aspects of fractal antenna. Asymmetric geometrical fractal shape and its optimization is the novel feature of the presented antenna. In this motif, frequency as well as time domain analysis is done and optimized results are presented. All these aforesaid features of this antenna is defined in detail in the upcoming sections of the paper. Section 2 discusses the designing aspects of the antenna and its evolution. Sections 3 and 4 analyze antenna's performance in frequency and time domain respectively Last Sect. 5

constitutes a comparative study of contemporary and relevant state of art with presented structure along with conclusion.

2 Design and development of the antenna

Every advent in technology is a quintessential outcome of designing and fabricating efficient components of the system. In present scenario, contemplation of nm structures is possible due to evolution in fabrication techniques. Availability of high resolution top-down lithography processes like scanning probe lithography and nano-sphere lithography, makes it feasible to design miniaturized structures of nm range. Chemical vapor deposition method represents bottom-up approach of fabrication and is very much suited for noble metals (Alejandro and Beser 2016). Figure 1a shows the geometry of the initiator patch antenna. It is designed by using 50 Ω fed microstrip line of length $L_m \times W_m$ on the ground plane of $L_g \times W_s$. Presented antenna is designed with silicon dioxide as a substrate with a height of 1.6 mm and relative permittivity of $\varepsilon_r = 3.8$. Designing process of any antenna starts with choosing operating resonant frequency of the antenna which is followed by selection of materials that can be used at that particular frequency range. Material choice at THz frequency range, is a profound process which have a direct impact on antenna performance. Silver is chosen to etch patch on SiO_2 substrate due to smallest dissipative losses offered among all metals (Lepeshov et al. 2018) and ease in epitaxial grown single crystalline thin films (Rodionov et al. 2019).

Operating frequency of any patch antenna characteristically depends upon width, length and dielectric constant of the substrate taken. We are taking a square patch as initiator or zeroth iteration of the fractal patch antenna hence $W = L$ is considered.

$$L = \frac{C}{2f_o\sqrt{\varepsilon}},\tag{1}$$

$$\varepsilon_{\text{reff}} = \frac{\varepsilon_r + 1}{2} + \frac{\varepsilon_r - 1}{2}\left[\frac{1}{\sqrt{1 + \frac{12h}{L}}}\right].\tag{2}$$

Effective length can be varied by varying $\varepsilon_{\text{reff}}$ by altering ε_r, as given below
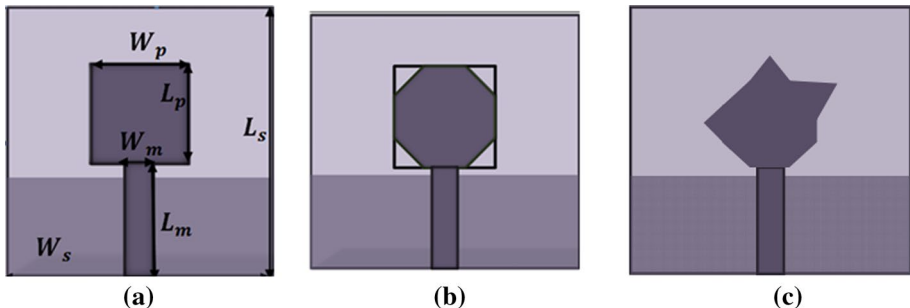

Fig. 1 **a** Geometry of Iteration 0, **b** Iteration 1 and **c** Iteration 2 respectively

$$L = \frac{c}{2f_0\sqrt{\varepsilon_{reff}}}. \tag{3}$$

Fringe factor ΔL can be calculated by following equation

$$\Delta L = 0.412\frac{\left(\varepsilon_{reff} + 0.3\right)\left(\frac{L}{h} + 0.262\right)}{\left(\varepsilon_{reff} - 0.258\right)\left(\frac{L}{h} + 0.813\right)}. \tag{4}$$

Therefore, the actual length of the micro strip patch antenna is given as

$$L = L_{eff} - 2\Delta L. \tag{5}$$

In first designing phase a square patch is designed using Eqs. (1)–(5) and later alterations in the dimensions of antenna are done to improve radiation properties of antenna by using CST 3D simulator. At initiator dimensions of patch are $L_p = 18$mm and $W_p = 18$mm for dual band operation with a ground plane of $L_g \times W_s$ as shown in figure below.

In Iteration 1, as shown in Fig. 1b, right angle isosceles triangle (RIT) with $s1 = 4$µm is etched off from all four corners of square patch of initiator, which converts the geometry of patch into octagon. Octagon shape reduces the area and increases the impedance bandwidth of the proposed structure. Reducing the area or space filling property of fractal antenna, enhance the overall radiation characteristics of antenna. Octagon shape constitutes the intermediate stage of the antenna (Table 1).

Figure 1c shows the geometry of proposed irregular and asymmetric patch antenna. As shown in Fig. 2a, b, an acute isosceles triangles (AIT) along with one RIT, are added to the sides of octagon in such a manner so that it can generate multiple mode resonances to achieve super wide bandwidth. Indentation angle $\alpha = 60$ is taken for AIT triangle is added at upper branch of the octagon while RIT is added to the side branch of patch.

A better physical insight in the geometry of proposed asymmetric and irregular polygon can be achieved with the help of vertices in X–Y plane of antenna as shown in Fig. 2c. Position of vertices and triangles amalgamation in generator state of patch antenna is depicted in Table 2.

2.1 Frequency domain analysis of reported antenna

In this letter, modified Koch curve is presented which shows immaculate mathematical attributes with self-similarity and space filling properties. Mathematically, Koch fractal geometries can be best explained with fractal similarity dimension (Gupta and Mathur 2018) given as:

Table 1 The dimensions of the antenna structure (units of dimensions is µm)

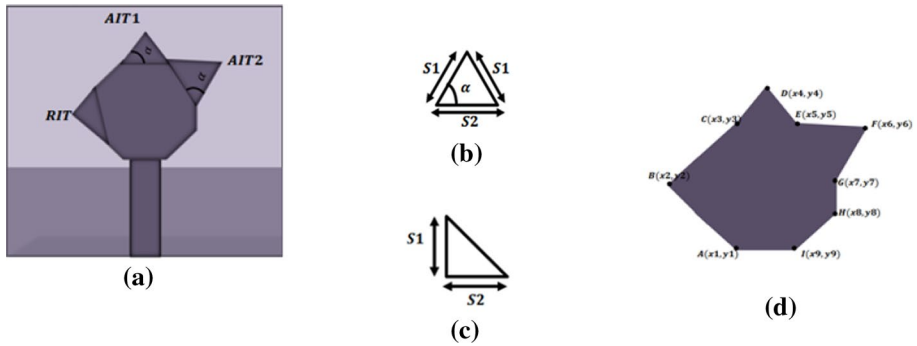| Parameter	Dimensions	Parameter	Dimensions
L_g	15	W_g	40
W_m	4	L_m	20
L_s	40	W_s	40
H_s	1.6	L_p	18
W_p	18		

(a)

(b)

(c)

(d)

Fig. 2 **a** Iteration 2 with inserted AIT and RIT, **b** AIT, **c** RIT and **d** patch represented in form of vertices

Table 2 The dimensions of the irregular polygon patch (in form of position coordinates) (units of dimensions is μm)

Parameter	Value	Parameter	Value	Parameter	Value	Parameter	Value
x_1	− 5	y_1	− 5	x_7	13	y_7	13
x_2	− 13	y_2	1	x_8	9	y_8	7
x_3	− 5	y_3	13	x_9	9	y_9	1
x_4	− 3	y_4	13	x_{10}	5	y_{10}	− 5
x_5	− 3	y_5	17	s_1	4	s_2	8
x_6	5	y_6	13				

$$FD = \frac{\log N}{\log \frac{1}{\varepsilon}}, \tag{6}$$

where N is total number of distinct copies or iterations, $\frac{1}{\varepsilon}$ is reduction factor value indicating change in length of new side with respect to original side length.

In presented case $N = 3$ and $\frac{1}{\varepsilon} = 3$, hence fractal similarity dimension is calculated as 1.

Evolution of antenna in terms of return loss and gain is depicted in Fig. 3a, b. At initiator or Iteration 0, which is a square patch antenna, behavior of antenna can be summarized as a dual band antenna radiating for 2.9–4.6 THz and 7.5–9.2 THz band. Maximum gain obtained in this iteration is 4.6 in its operating bandwidth. In Iteration 1, where an octagon is developed after chipping off four RIT from all corners of square patch. Due to introduction of higher order modes in octagon, antenna is radiating as wideband antenna from 2.9–4.5 THz, 6.6–8.5 THz, 9.2–15.3 THz with a peak gain of 5.3. Improved radiation characteristics of antenna are resulted from the introduction of edges in the geometrical structure of the antenna. Edges alter the current path which in turn modify the characteristics of antenna (Yadav and Tripathi 2013). In generator or Iteration 2, further edges are increased. Two AIT and one RIT is added which yields further higher order *TM* modes which combined together to give a super wide operating bandwidth. Maximum gain obtained in this iteration of antenna is 6 dB which increases the practical viability of antenna.

In this work, a novel fractal approach for designing of patch is opted, so that with application of fractal geometry multiple resonances can be excited. With every successive iteration, alterations in the geometry results in higher order *TM* mode generation, which yields
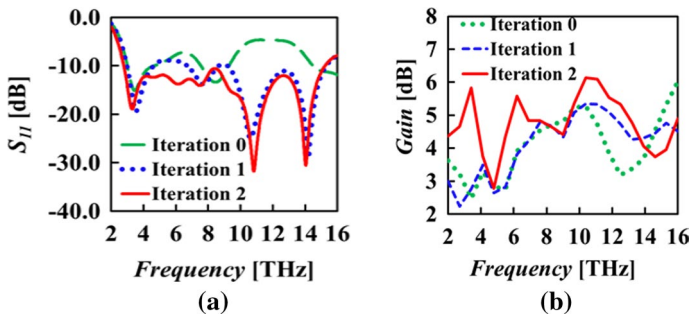
Fig. 3 **a** Return loss of successive iterations and **b** comparative gain among three iterations

multiple resonances. Amalgamation of these resonance resulted in super wide bandwidth. Figure 4a represents voltage standing wave ratio of the antenna. At a scale of 2:1, antenna bandwidth is obtained from 2.7 to 15.2 THz. Impedance plot of the antenna is shown by Fig. 4b which depicts variations in the impedance of the radiator in the operating band of the antenna. As indicated probably five TM modes exist in the antenna to make it a ultra wide band antenna. These modes exist at frequency of 2.8, 4.8, 8.8, 11.8 and 13.7 THz as can be observed from the impedance curve. Figure 4a represents voltage standing wave ratio of the antenna. At a scale of 2:1, antenna bandwidth is obtained from 2.7 to 15.2 THz. Impedance plot of the antenna is shown by Fig. 4b which depicts variations in the impedance of the radiator in the operating band of the antenna.

In this work, a novel fractal approach for designing of patch is opted, so that with application of fractal geometry multiple resonances can be excited. With every successive iteration, alterations in the geometry results in higher order *TM* mode generation, which yields multiple resonances. Figure 5 represents surface current distribution of rectangle geometry (Iteration 0) of presented antenna. In this iteration, uppermost edges in both right and left direction are almost not radiating. At lower frequencies, low value of surface current still exists that can be visualized via Fig. 5a, b. However, as the frequency increases surface current on upper edges almost vanishes as can be observed from Fig. 5c–e.

Figure 6 represents surface current distribution of the second evolution stage of presented antenna structure. Figure 6a displays current distribution at lowest *TM* mode resonating at 2.7 THz. Further modes are generated at 3.6, 5.8 and 8.6 THz and it can be observed from Fig. 6b–d that octagon edges contains maximum current consequences
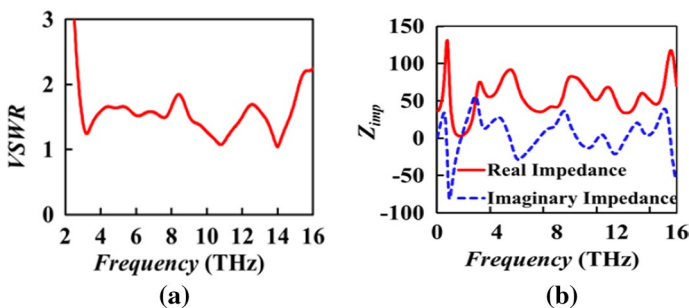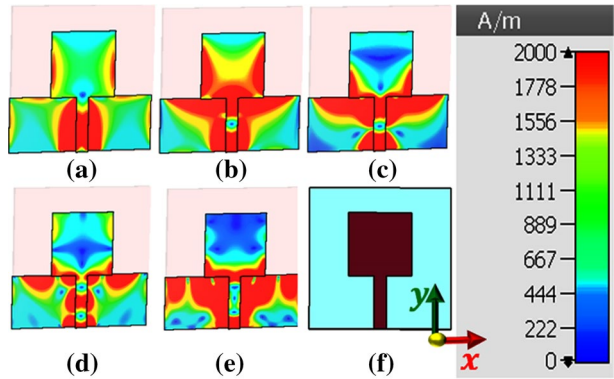

Fig. 4 **a** VSWR and **b** real and imaginary part of impedance of the proposed structure

Fig. 5 Surface current distribution in **Iteration 0 at a** 3 THz, **b** 4.4 THz, **c** 7.5 THz, **d** 10.9 THz and **e** 14.4 THz, **f** represents the geometry of the present structure at 0th iteration

in radiation. At further high frequencies 11.6, 13.4 and 15.2 THz combination of partial ground plane and microstrip feed creates higher order resonance. In this Iteration, electrical length of the antenna increase that results in lowest TM mode to be shifted from 3 to 2.8 THz. Further higher order frequency modes at 13.7 and 15.7 have been generated.

Figure 7 represents surface current distribution in Iteration 2. Multiple TM modes exist in the antenna at frequencies of 2.8, 4.8, 8.8, 11.3, 13.7 and 15.5 THz as can be observed from the impedance curve. Surface current distribution of the antenna is shown in Fig. 7 corresponding to these resonating frequencies. As it can be observed from Fig. 7 that current is mainly distributed around feed line, ground and edges of the reported patch antenna. This asymmetrical shape of presented nano antenna increase electrical length of the antenna at all frequencies radiated in Iteration 1. Lower order as well as higher order modes have been shifted towards left in the frequency response curve in Iteration 2. Extension of Koch borderline geometry results in enhanced currents. As frequency increases further from 2.8 higher order modes are generated which gives rise to generation of higher order harmonics in the patch antenna. It is evident from Fig. 7 that edges are radiating at lower as well as higher frequencies resulting in super wide bandwidth.
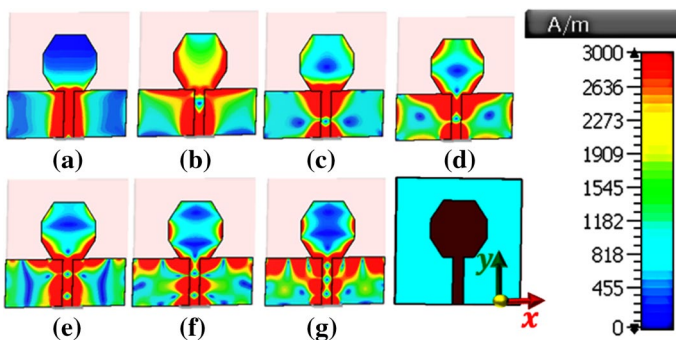

Fig. 6 Surface current distribution in **Iteration 1 at a** 2.7 THz, **b** 3.6 THz, **c** 5.8 THz, **d** 8.6 THz, **e** 11.6 THz, **f** 13.4 THz, and **g** 15.2 THz
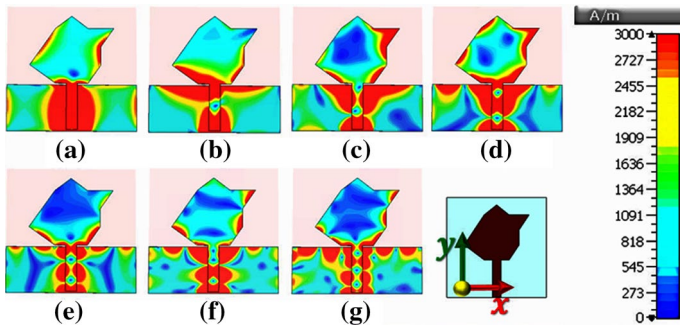
Fig. 7 Surface current distribution in **Iteration 2** at **a** 2.8 THz, **b** 4.8 THz, **c** 8.8 THz, **d** 9.5 THz, **e** 11.3 THz, **f** 13.7 THz, and **g** 15.5 THz

3 Parametric analysis

Figure 6 shows various simulations done to achieve a wide impedance bandwidth in second iteration. Koch curve is flared in all branches with the triangular approach as shown in Fig. 8a, and is resulted in non-radiating configuration of the radiator. In configuration (Fig. 8b–d) step by step addition of triangle is done to get the desired response. Inclusion of edges in a radiating structure influences the overall impedance of the antenna. Addition of sharp edges in a fractal antenna impacts either inductive or capacitive reactance in overall impedance parameter. In Fig. 8b, a single triangle is added at uppermost branch of the octagon which resulted in multiband structure as depicted in Table 3. Figure 8c has both flared side arms, while Fig. 8d has one side arm. It is interesting to note that addition of triangle in two side upper arms, doesn't match the impedance perfectly. Dual wide band antenna with frequency bands 2.9–3.9 and 6–15.6 GHz is obtained with single arm extension. This reason leads to removal of dual arm extension in design.

Figure 9 shows the axial ratio of the proposed structure. It is evident from the Fig. 9 that proposed antenna (PA) is a linearly polarized antenna.

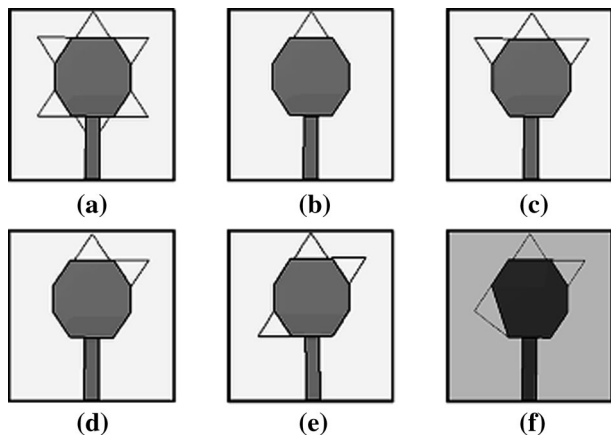**Fig. 8** Evolution stages of antenna

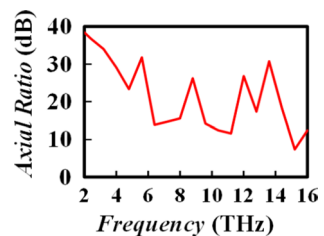**Table 3** Comparison of various simulated structures with proposed one

S. nos.	Configuration	Bandwidth
1	A	Non-radiating
2	B	2.9–3.9, 6–8, 9.8–15.7
3	C	2.9–3.9, 7.8–15.2
4	D	2.9–3.9, 6–15.6
5	E	3–8.4, 10–14.5
6	F	5.4–15

Figure 8e shows the modified lower arm triangle addition of the proposed structure. Same response has been observed when both lower branches were extended with addition of triangles. Hence one branch extension which enhances bandwidth is chosen which yields a dual bandwidth of 3.8–4 and 10–14.5 GHz. PA is shown in Fig. 8f and resulted after modifying acute isosceles triangle into right angle triangle. Phenomenon of electrical shortening is achieved by adding capacitive reactance in the total impedance which paves the patch of perfect impedance matching as can be observed from the impedance plot given in Fig. 4b.

4 Impact of ground on reflection coefficient of antenna

Cumulative response of ground structure with Koch fractal shape yields super wide bandwidth response of antenna. Return loss response of antenna structure is optimized using full wave simulator CST microwave studio. The length of the ground in PA is 15 μm and at this length it gives maximum bandwidth which is from 2.7 to 15.2 THz. When full length of the ground (FG) is taken (40 μm) then antenna behaves as multiband and operate on 3.3–3.8 THz, 8.2–8.5 THz and 10.8–11.7 THz. When length decreased to 20 μm, half ground (HG) then antenna operate between 12.4 and 17.7 THz due to impedance matching and thus antenna provides the wideband response and when further decreased to 10 μm quarter ground (QG), antenna does not radiate due to poor impedance matching. Hence it is concluded that at the length of 15 μm, antenna operates best. Figure 10b shows the comparison of S11-parameter response of antenna. Table 4 gives comparative measure of varying length of the ground. Peak gain, impedance bandwidth with maximum return loss obtained are the parameters which are tabulated and compared to see effect of ground on radiating properties of antenna.

Radiation pattern of any antenna determine extent of impedance matching and satisfactory return loss behavior of antenna. Figure 11 shows radiation pattern for multi-mode resonant

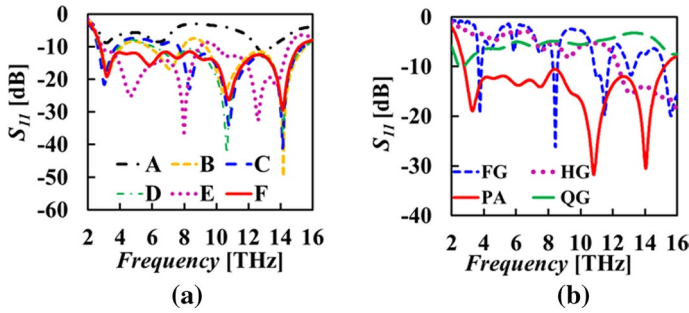**Fig. 9** Axial ratio of the proposed antenna

Fig. 10 **a** Reflection coefficient of various configurations simulated and **b** variations in ground structure

Table 4 Comparison of ground with varying length (dimension unit: μm)

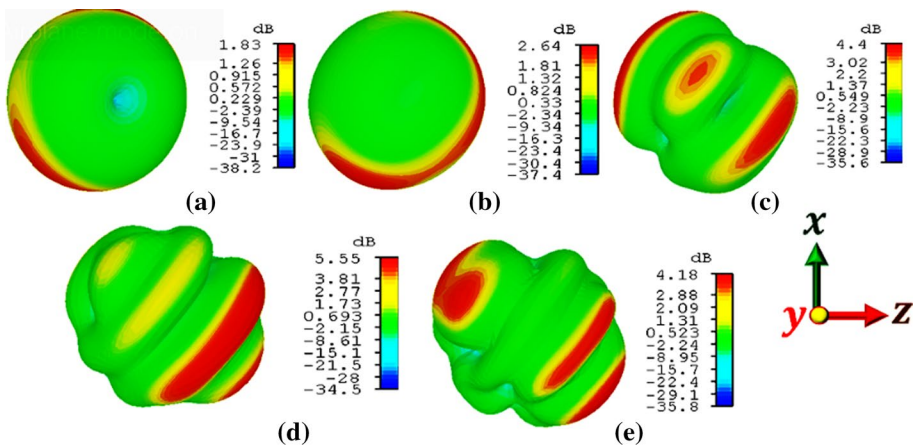| S. nos.	Antenna with ground structure	Bandwidth (THz)	Maximum reflection coefficient (dB)	Gain (dBi)
1	Full ground (FG)	Multiband 3.3–3.8, 8.2–8.5, 10.8–11.7	− 25 at 8.4	5.9
2	Half ground (HG)	12.4–17.7	− 17 at 16	5.7
3	Quarter ground (QG)	Not radiating	–	–
4	Proposed antenna (PA)	2.7–15.2	− 32 at 10.8	6.1

Fig. 11 Radiation pattern of antenna at frequency **a** 2.8 THz, **b** 4.8 THz, **c** 8.8 THz, **d** 11.4 THz, and **e** 13.7 THz

frequencies of antenna. Figure 11a shows a perfect monopole radiation pattern. It is interesting to note that for low frequency, antenna is radiating as perfect monopole antenna. E-plane and H-plane both displays broadband radiation patterns with low side lobe levels. But with increase in frequency, higher order harmonics are generated. These high frequency electromagnetic fields constitute scattering of energy in different directions which resulted in multiple lobes. Hence for lower frequency range, perfect monopole radiations patterns are obtained, but

as frequency increases multiple lobe radiation patterns are obtained due to higher order harmonics. This type of radiation pattern is highly suitable for microwave imaging applications.

Radiation efficiency and gain obtained by the antenna is given in Fig. 12a and b, respectively. At THz frequency range high attenuation losses occurs in metallic radiators. Skin depth is also a major cause of reduction in efficiency of the patch antenna. Average efficiency achieved in overall operating bandwidth of antenna is 85% which is a quite good value for practical usage of antenna. Gain v/s frequency characteristics are shown in Fig. 12 that gives peak gain of 6 dB at a frequency of 10.3 THz. High gain with super wide band efficiency makes design highly suitable for spectroscopy and THz microwave imaging applications.

5 Time domain analysis of antenna

Time domain analysis of antenna utilizing short pulses in UWB systems is significant due to its high efficiency electromagnetic wave transmission and high resolution to interrogate the targets (Shlivinski 1997) in wireless communication. Impulse transmission is a cost effective method of exchanging information. This technology doesn't make use of carrier, which enables these wireless systems to have simple transceiver architecture. Gaussian monocycle or one of its derivative are send as UWB pulse which is easy to generate. Time domain analysis of any wide band antenna system is necessary in order to verify its pulse preserving capabilities (Wu et al. 2008; Kwon 2006). The factor used to authenticate the relationship between input and output pulse is known as fidelity factor. Fidelity factor represents the highest magnitude of cross correlation between transmitted and received pulse. The time domain characteristics of monopole antennas discussed in this paper are calculated with the help of CST Microwave Studio. Pulse preserving capabilities of these antennas are evaluated in the scope of correlation factors which measure correlation between the input pulse signal and the electric field intensity signals in their far field region.

UWB signal is the fifth-derivative of the Gaussian pulse and is given by equation:

$$s_1(t) = GM_5(t) = C\left(-\frac{t^5}{\sqrt{2\pi}\sigma^{11}} + \frac{10t^3}{\sqrt{2\pi}\sigma^9} - \frac{15t}{\sqrt{2\pi}\sigma^7}\right) \times \exp\left(-\frac{t^2}{2\sigma^2}\right), \qquad (7)$$

where C is a constant which can be chosen to comply with the peak power spectral density suggested by FCC and σ has to be 51 ps to ensure that the shape of the spectrum complies with the FCC spectral mask. By placing some virtual probes at a distance of 67 μm away
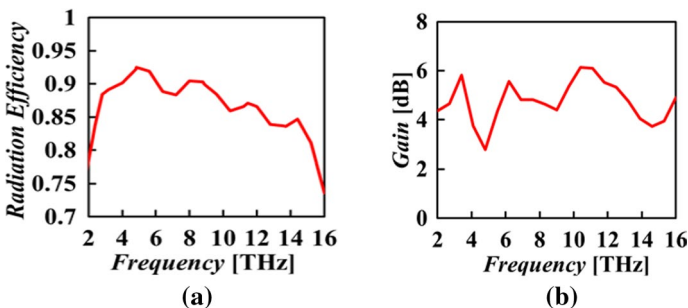

Fig. 12 a Radiation efficiency and **b** gain of antenna

from the feed point of monopole antenna, the corresponding Eθ components of electric field intensity signal $s_2(t)$ could be readily obtained. We can calculate the correlation factors to evaluate the pulse preserving capabilities of these antennas as follows:

$$\rho = max\left\{\frac{\int s_1(t)s_2(t-\tau)dt}{\sqrt{\int s_1^2(t)dt}\sqrt{s_2^2(t)dt}}\right\}, \tag{8}$$

where τ is the delay to maximize ρ in above equation.

The simulated correlation factors of the presented antennas are calculated for two side and one face to face configuration for different probe position in terms of θ and ϕ. Maximum correlation factor among all values is defined as fidelity for a particular direction. In proposed research, we have only simulated probes in three configuration by keeping θ = 90° and varying value of ϕ from 0° to 90°.

This work devises three arrangements of invigilating reciprocation of short input pulse and measuring fidelity. Two side by side (S by S) in X and Y-direction (Fig. 13a, b) and a face to face (F to F) method in Z-direction (Fig. 13c), a default Gaussian pulse is generated in CST Microwave Studio which travels across the entire operating band is taken as input signal. According to arrangement in which we are measuring, probes are inserted at a distance of $2D^2/\lambda$ μm.

It is interesting to observe here that for all three setups waveforms received are similar to transmitted pulses except marginal spreading being observed in S by S (X-axis). If we analyse side radiation in X-direction, waveform is little bit distorted and inequality in the magnitude of both transmit and received pulse is also observed. Simulated fidelity factor calculated for S by S (X-axis) is 0.7264 while for Y-axis it is 0.9537. Highest fidelity factor of 0.9597 is achieved in Face to face configuration which is a measure of accuracy of shape preserving capability of pulse. In TPI and TPS systems, for short distance communication, amplitude and phase information obtained by time domain analysis is used to create 3D images.

Figure 13d represents the simulated group delay function of the entire system. Group delay represents the signal phase distortion of the signal travelling through ultra wide bandwidth. From Fig. 13d it can be observed that an almost steady response of group delay is obtained by proposed structure except at frequency of 11 and 14 THz. Higher order harmonics causes distortion in phase of the signal. To conclude, it is notable that presented antenna is a small size, super wide bandwidth, high gain antenna which has high efficiency and satisfactory group delay.

6 Comparison of presented paper with contemporary work

Table 5 shows a comparison amongst metallic patch antennae which have already been proposed in literature. As can be seen from the table the dimensions of reported antenna have scale down approximately 8 to 10 times as compare to other entries of the table. Bandwidth achieved with this super compact design is 12.5 THz and a peak gain of 6 dB is achieved. To best of author's knowledge this is the maximum bandwidth achieved by any metallic radiator till date. Hence for compact size, high bandwidth and high gain requirement this antenna is best suited.
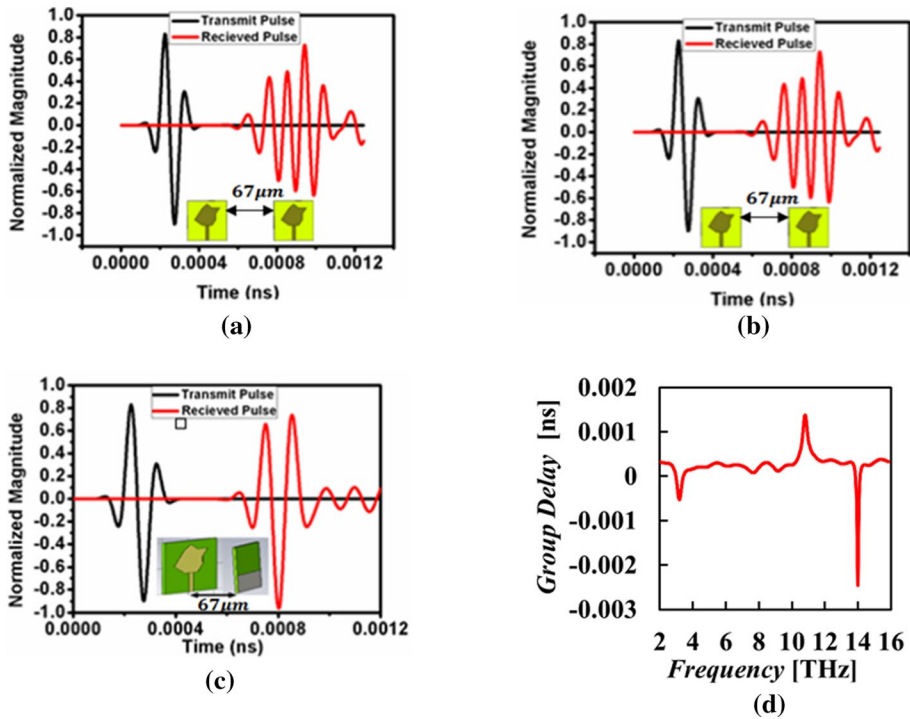
Fig. 13 Normalized magnitude of three different arrangements. **a**, **b** Side by side in X and Y direction and **c** in Z-direction. **d** Cumulative group delay

7 Conclusion

A modified Koch frontier patch antenna providing super wide bandwidth of 12.5 THz with a high gain of 6 dB is presented in this paper. Presented design is a unique combination of metallic patch and partial ground structure. In frequency domain analysis, impedance bandwidth of 139% with the range 2.7–15.2 THz is achieved with reducing the length of the ground. Irregular octagon is parametrically analysed with internal angle of a particular side and its impact on gain and frequency is carefully examined. Monopole radiation patterns and peak gain of 6.1 dB is achieved throughout the resonating band which makes this design perfectly suitable to mitigate high attenuation of THz regime. Silver is chosen as material for patch fabrication due to its lowest dispersive loss offered among all metals. In time domain analysis, three paradigms are taken when antenna is placed in all X, Y and Z-direction from its base value. High fidelity factor of 0.9597 is achieved in face to face configuration which makes antenna most suited for super wide band communication. Compactness and simplicity of design, ease in fabrication and excellent characteristics makes it suitable generator and receiver for THz imaging and spectroscopy.

Table 5 Comparison with other broadband THz antennas

S. nos.	Dimensions (λ^3)	Shape of patch	Patch material	Substrate material	Gain (dB)	Bandwidth (THz)
Jha and Singh (2009)	$0.4\lambda_0 \times 0.5\lambda_0 \times .045\lambda_0$	Rectangular	PEC	Silicon di oxide	6.5	14.24 (4.76–19)
Singhal (2019a)	$2.47\lambda_0 \times 2.479\lambda_0 \times 0.011\lambda_0$	Fractal circular	Copper	Polyamide	12.89	9.9 (0.1–10)
Singhal (2019b)	$12\lambda_0 \times 9\lambda_0 \times 1.2\lambda_0$	Elliptical	Copper	Polyamide	9.5	9 (0.3–9.3)
Das et al. (2020)	$6.6\lambda_0 \times 5\lambda_0 \times 0.67\lambda_0$	Elliptical	Copper	Polyamide	12	5 (0.46–5.46)
Das and Rawat (2021)	$0.168\lambda_0 \times 0.168\lambda_0 \times 0.022\lambda_0$	Hexagonal	Graphene	Quartz	7.99	0.95 (0.68–1.63)
Shamim et al. (2021)	$0.74\lambda_0 \times 0.74\lambda_0$	Rectangle with dual stub	Copper	Polyamide	16.48	7.47 (0.53–8)
This antenna	$0.79\lambda_0 \times 0.79\lambda_0 \times 0.032\lambda_0$	Asymmetric polygon	Silver	Silicon di-oxide	6	12.5 (2.7–15.2)

Declarations

Conflict of interest The authors have not disclosed any competing interests.

References

Akyildiz, I.F., Jornet, J.M.: Realizing ultra-massive MIMO (1024 × 1024) communication in the (0.06–10) terahertz band. Nano Commun. Netw. **8**, 46–54 (2016). https://doi.org/10.1016/j.nancom.2016.02.001

Akyildiz, I.F., Jornet, J.M., Han, C.: Terahertz band: next frontier for wireless communications. Phys. Commun. **12**, 16–32 (2014). https://doi.org/10.1016/j.phycom.2014.01.006

Alejandro, N., Beser, S.: Nanotechnology Fabrication Methods, pp. 1–15 (2016)

Bala, R., Marwaha, A.: Characterization of graphene for performance enhancement of patch antenna in THz region. Optik (Stuttg.) **127**(4), 2089–2093 (2016). https://doi.org/10.1016/j.ijleo.2015.11.029

Cheng, J., Fan, F., Chang, S.: Recent progress on graphene-functionalized metasurfaces for tunable phase and polarization control. Nanomaterials (2019). https://doi.org/10.3390/nano9030398

Das, V., Rawat, S.: Modified rectangular planar antenna with stubs and defected ground structure for THz applications. Optik (Stuttg.) **242**, 167292 (2021). https://doi.org/10.1016/j.ijleo.2021.167292

Das, S., Mitra, D., Ranjan, S., Chaudhuri, B.: Fractal loaded circular patch antenna for super wide band operation in THz frequency region. Optik Int. J. Light Electron Opt. (2020). https://doi.org/10.1016/j.ijleo.2020.165528

Denizhan Sirmaci, Y., Akin, C.K., Sabah, C.: Fishnet based metamaterial loaded THz patch antenna. Opt. Quantum Electron. **48**(2), 1–10 (2016). https://doi.org/10.1007/s11082-016-0449-6

Formanek, F., Brun, M.A., Umetsu, T., Omori, S., Yasuda, A.: Aspheric silicon lenses for terahertz photoconductive antennas. Appl. Phys. Lett. **94**(2), 23–26 (2009). https://doi.org/10.1063/1.3072357

Galoda, S., Singh, G.: Fighting terrorism with terahertz. IEEE Potentials **26**(6), 24–29 (2007). https://doi.org/10.1109/MPOT.2007.906117

Goyal, R., Vishwakarma, D.K.: Design of a graphene-based patch antenna on glass substrate for high-speed terahertz communications. Microw. Opt. Technol. Lett. **60**(7), 1594–1600 (2018). https://doi.org/10.1002/mop.31216

Grade, J., Haydon, P., Van Der Weide, D.: Electronic terahertz antennas and probes for spectroscopic detection and diagnostics. Proc. IEEE **95**(8), 1583–1591 (2007). https://doi.org/10.1109/JPROC.2007.898900

Guo, L., Huang, F., Tang, X.: A novel integrated MEMS helix antenna for terahertz applications. Optik (Stuttg.) **125**(1), 101–103 (2014). https://doi.org/10.1016/j.ijleo.2013.06.016

Gupta, D.M., Mathur, V.: Koch boundary on the square patch microstrip antenna for ultra wideband applications. Alex. Eng. J. **57**(3), 2113–2122 (2018). https://doi.org/10.1016/j.aej.2017.06.005

Jha, K.R., Singh, G.: Improved performance analysis of square patch microstrip antenna at terahertz frequency. In: ARTCom 2009—International Conference on Advances in Recent Technologies in Communication and Computing, pp. 676–679, 2009. https://doi.org/10.1109/ARTCom.2009.16

Jha, K.R., Singh, G.: Analysis and design of rectangular microstrip antenna on two-layer substrate materials at terahertz frequency. J. Comput. Electron. **9**(2), 68–78 (2010). https://doi.org/10.1007/s10825-010-0306-y

Jha, K.R., Singh, G.: Analysis and design of terahertz microstrip antenna on photonic bandgap material. J. Comput. Electron. **11**(4), 364–373 (2012). https://doi.org/10.1007/s10825-012-0416-9

Koenig, S., et al.: Wireless sub-THz communication system with high data rate. Nat. Photonics **7**(12), 977–981 (2013). https://doi.org/10.1038/nphoton.2013.275

Kucherik, A., et al.: Nano-antennas based on silicon–gold nanostructures. Sci. Rep. **9**(1), 1–6 (2019). https://doi.org/10.1038/s41598-018-36851-w

Kwon, D.H.: Effect of antenna gain and group delay variations on pulse-preserving capabilities of ultra wideband antennas. IEEE Trans. Antennas Propag. **54**(8), 2208–2215 (2006). https://doi.org/10.1109/TAP.2006.879189

Lepeshov, S., et al.: Boosting terahertz photoconductive antenna performance with optimised plasmonic nanostructures. Sci. Rep. **8**(1), 1–7 (2018). https://doi.org/10.1038/s41598-018-25013-7

Luk, K.M., et al.: A microfabricated low-profile wideband antenna array for terahertz communications. Sci. Rep. **7**(1), 1–11 (2017). https://doi.org/10.1038/s41598-017-01276-4

Mathur, V., Gupta, D.M.: Morphology of Koch fractal antenna. Int. J. Comput. Technol. **13**(2), 4157–4163 (2014). https://doi.org/10.24297/ijct.v13i2.2902

Mirmosaei, S.S., Afjei, S.E., Mehrshahi, E., Fakharian, M.M.: A dual band-notched ultra-wideband monopole antenna with spiral-slots and folded SIR-DGS as notch band structures. Int. J. Microw. Wirel. Technol. **8**(8), 1197–1206 (2016). https://doi.org/10.1017/S1759078715000719

Nafari, M., Jornet, J.M.: Metallic plasmonic nano-antenna for wireless optical communication in intra-body nanonetworks. In: BodyNets International Conference on Body Area Networks, 2015. https://doi.org/10.4108/eai.28-9-2015.2261410

Obayya, S., Hameed, F.O.M., Fayez Fahmy, N., Hussein Abdelrazik, M.: Optical nano-antennas for energy harvesting, May 2018. https://doi.org/10.4018/978-1-5225-1671-2.ch006

Pickwell, E., Wallace, V.P.: Biomedical applications of terahertz technology. J. Phys. D (2006). https://doi.org/10.1088/0022-3727/39/17/R01

Rodionov, I.A., et al.: Quantum engineering of atomically smooth single-crystalline silver films. Sci. Rep. **9**(1), 1–9 (2019). https://doi.org/10.1038/s41598-019-48508-3

Seyedsharbaty, M.M., Sadeghzadeh, R.A.: Antenna gain enhancement by using metamaterial radome at THz band with reconfigurable characteristics based on graphene load. Opt. Quantum Electron. **49**(6), 1–13 (2017). https://doi.org/10.1007/s11082-017-1052-1

Shamim, S.M., Das, S., Hossain, M.A., Madhav, B.T.P.: Investigations on graphene-based ultra-wideband (UWB) microstrip patch antennas for terahertz (THz) applications. Plasmonics (2021). https://doi.org/10.1007/s11468-021-01423-8

Shanawani, M., Masotti, D., Costanzo, A.: THz rectennas and their design rules. Electronics (2017). https://doi.org/10.3390/electronics6040099

Sharma, T., Varshney, G., Yaduvanshi, R.S., Vashishath, M.: Obtaining the tunable band-notch in ultra wideband THz antenna using graphene nanoribbons. Opt. Eng. **59**(04), 1 (2020). https://doi.org/10.1117/1.oe.59.4.047103

Shlivinski, A.: Antenna characterization in the time domain. IEEE Trans. Antennas Propag. **45**(7), 1140–1149 (1997). https://doi.org/10.1109/8.596907

Singhal, S.: Ultra wideband elliptical microstrip antenna for terahertz applications. Microw. Opt. Technol. Lett. (2019a). https://doi.org/10.1002/mop.31910

Singhal, S.: Elliptical ring terahertz fractal antenna. Optik (Stuttg.) **194**(3), 163129 (2019b). https://doi.org/10.1016/j.ijleo.2019.163129

Son, J.H.: Terahertz electromagnetic interactions with biological matter and their applications. J. Appl. Phys. (2009). https://doi.org/10.1063/1.3116140

Unal, G.S., Aksun, M.I.: Bridging the gap between RF and optical patch antenna analysis via the cavity model. Sci. Rep. **5**, 1–8 (2015). https://doi.org/10.1038/srep15941

Varshney, G., Gotra, S., Pandey, V.S., Yaduvanshi, R.S.: Proximity-coupled graphene-patch-based tunable single-/dual-band notch filter for THz applications. J. Electron. Mater. (2019). https://doi.org/10.1007/s11664-019-07274-8

Werner, D.H., Ganguly, S.: An overview of fractal antenna engineering research. IEEE Antennas Propag. Mag. **45**(1), 38–57 (2003). https://doi.org/10.1109/MAP.2003.1189650

Wu, Q., Jin, R., Geng, J.: Pulse preserving capabilities of printed circular disk monopole antennas with different substrates. Prog. Electromagn. Res. **78**(10), 349–360 (2008). https://doi.org/10.2528/PIER07092004

Xu, Z., Dong, X., Bornemann, J.: Design of a reconfigurable MIMO system for THz communications based on graphene antennas. IEEE Trans. Terahertz Sci. Technol. **4**(5), 609–617 (2014). https://doi.org/10.1109/TTHZ.2014.2331496

Yadav, S., Tripathi, S., Mohan, A.: A compact octagonal-shaped fractal UWB antenna with Sierpinski fractal geometry. Microw. Opt. Technol. Lett. **55**(11), 2562–2568 (2013). https://doi.org/10.1002/mop

Publisher's Note Springer Nature remains neutral with regard to jurisdictional claims in published maps and institutional affiliations.